Application of empirical mode decomposition to heart rate variability analysis

J. C. Echeverría[1,2] J. A. Crowe[1] M. S. Woolfson[1] B. R. Hayes-Gill[1]

[1]School of Electrical & Electronic Engineering, University of Nottingham, Nottingham, UK
[2]Electrical Engineering Department, Universidad Autónoma Metropolitana-Izt., Mexico

Abstract—*The analysis of heart rate variability, involving changes in the autonomic modulation conditions, demands specific capabilities not provided by either parametric or non-parametric spectral estimation methods. Moreover, these methods produce time-averaged power estimates over the entire length of the record. Recently, empirical mode decomposition and the associated Hilbert spectra have been proposed for non-linear and non-stationary time series. The application of these techniques to real and simulated short-term heart rate variability data under stationary and non-stationary conditions is presented. The results demonstrate the ability of empirical mode decomposition to isolate the two main components of one chirp series and three signals simulated by the integral pulse frequency modulation model, and consistently to isolate at least four main components localised in the autonomic bands of 14 real signals under controlled breathing manoeuvres. In addition, within the short time–frequency range that is recognised for heart rate variability phenomena, the Hilbert amplitude component ratio and the instantaneous frequency representation are assessed for their suitability and accuracy in time-tracking changes in amplitude and frequency in the presence of non-stationary and non-linear conditions. The frequency tracking error is found to be less than 0.22% for two simulated signals and one chirp series.*

Keywords—*Heart rate variability, Empirical mode decomposition, Hilbert transform, Non-linearity, Non-stationarity*

Med. Biol. Eng. Comput., 2001, **39**, 471–479

1 Introduction

THE AUTONOMIC control mechanisms of cardiac function are involved in short-term fluctuations in the time interval between consecutive heart beats (STEIN and KLEIGER, 1999; TASK FORCE, 1996). This phasic modulated phenomenon, which has been extensively studied (STEIN and KLEIGER, 1999), is conventionally referred to as heart rate variability (HRV) (TASK FORCE, 1996), with the power spectral distribution of the HRV reflecting autonomic chronotropic modulation (ECHEVERRÍA *et al.*, 1997) and respiratory activity (BROWN *et al.*, 1993). Consequently, power spectral analysis of short-term HRV, adopted for the evaluation of autonomic function (STEIN and KLEIGER, 1999; TASK FORCE, 1996), quantifies the sensitivity of the heart to modulation and can be used to make inferences about the dynamic conditions of the central oscillators, the sympathetic and vagal efferent activity and the sinus node (TASK FORCE, 1996). For example, reduced power in the short-term heart rate variability could suggest a deficiency in the central control of the heart rate, or a diminished response in the sinus node (STEIN and KLEIGER, 1999).

Correspondence should be addressed to J. C. Echeverría; e-mail: jcea@xanum.uam.mx

First received 9 November 2000 and in final form 18 April 2001
MBEC online number: 20013592

Three main spectral components have been identified in the HRV spectra calculated from short-term recordings of 2–5 min. These are a very low-frequency component (VLF) below 0.04 Hz; a low-frequency (LF) component, from 0.04 Hz to 0.15 Hz; and a high-frequency (HF) component, from 0.15 Hz to 0.4 Hz (TASK FORCE, 1996).

The physiological information provided by the VLF is dubious and not well established (TASK FORCE, 1996). In contrast, the efferent vagal activity is a major contributor to the power of the HF component (TASK FORCE, 1996), whereas disagreement exists about the interpretation of the LF component. Some studies suggest that the measuring of its power can be used as a quantitative marker for sympathetic modulations (if expressed in normalised units), and other studies indicate that the LF reflects both sympathetic and vagal activity (TASK FORCE, 1996). This latter hypothesis has led to the fractional power ratio between the low-frequency band and the high-frequency band in the HRV spectra being adopted by some investigators as an index of either the sympatho/vagal balance or sympathetic modulations (TASK FORCE, 1996).

Nevertheless, ECKBERG (1996), in an extensive review, has challenged the notion that the linear increase in sympathovagal balance that occurs during upright tilt reflects a shift of autonomic predominance from vagal to sympathetic mechanisms, together with the justification of extrapolating this to other circumstances. According to ECKBERG (1996),

the sympathovagal balance concept imposes non-existent attributes on the physiological regulatory mechanisms.

Furthermore, recent studies did not detect an increase in the LF R-R interval power in response to steadily increasing fluctuations of muscle sympathetic activity achieved by progressive tilt positions during controlled breathing (COOKE *et al.*, 1999). This finding has been used as a strong argument against the application of the LF power in the R-R interval spectra as a non-invasive index of sympathetic nerve activity (COOKE *et al.*, 1999; KARAMEKER, 1999), with the authors suggesting that the origin of the LF oscillations is localised in some pacemaker, possibly in the central nervous system, rather than in the baroreflex. In addition, within the same study, the respiratory fluctuations of the R-R intervals were found to decrease in proportion to the tilt angle. Both results suggest that tilt systematically reduces the respiratory gating of sympathetic and vagal motoneurone responsiveness to stimulatory inputs (COOKE *et al.*, 1999).

The HRV power spectral density is usually calculated by either non-parametric spectral methods (e.g. windowed FFT), or by parametric spectral methods (e.g. autoregressive modelling) (TASK FORCE, 1996). In general, these linear methods generate comparable results (TASK FORCE, 1996), but assume stationary conditions that are difficult to achieve even in short-term records under physiologically stable or autonomic controlled conditions. Ideally, the modulating mechanism of the heart rate should not change during the recording, so that the individual spectral components are attributed to specific physiological conditions (TASK FORCE, 1996). Consequently, these spectral methods produce time-averaged estimates of the power over the entire length of the record (SCHECHTMAN *et al.*, 1988; SHIN *et al.*, 1989). Therefore analysis of the transient physiological phenomena, involving changes in the modulation conditions, demands specific capabilities not provided by the above linear spectral methods (TASK FORCE, 1996).

Time-variant algorithms of autoregressive identification have been used to estimate the spectral characteristics of the HRV in correspondence to transient phenomena (MAINARDI *et al.*, 1995). For the analysis of the changes in the autonomic regulation, peak/trough and complex demodulation methods have also been proposed, allowing the description of the amplitude of selected frequency components as a function of time (SCHECHTMAN *et al.*, 1988; SHIN *et al.*, 1989).

Another limitation of the linear spectral methods is imposed by the irregularity of the HRV. As the trends of decreasing or increasing R-R intervals are not symmetrical, the estimated peak at the fundamental frequency is reduced (TASK FORCE, 1996). Moreover, the existence of an LF component in the HRV power spectrum, which disturbs the power quantification of the autonomic components, has also been recognised. Although generally associated with, and more evident in, long-term records, the presence of this component has been detected in short-term records, beginning at 10 s and lasting no more than 12 min (KOBAYASHI and MUSHA, 1982; SAUL *et al.*, 1988; YAMAMOTO and HUGHSON, 1991; CHAN *et al.*, 1997).

Recently, the empirical mode decomposition (EMD) method and the associated Hilbert spectra have been presented for the time-frequency adaptive analysis of non-linear and non-stationary time series (HUANG *et al.*, 1998). This decomposition has the advantage of automatically identifying the intrinsic time scales of the data, including the longest scale (i.e. the longer period oscillations) defined by the full length of the series, without any presuppositions regarding the data's form. Hence, the components derived from the decomposition may carry actual physical significance (HUANG *et al.*, 1998).

Given the described nature of HRV series data, it would appear that the EMD is a suitable and attractive method of analysis. Specifically, it may overcome the current difficulty of achieving strictly stationary conditions, be appropriate to reflect the non-linear contents of the data, and may allow the study of the frequency information carried by the series as a function of time. This paper presents the application of the EMD and Hilbert transform, first, to a set of simulated HRV series produced by the integral pulse frequency modulation (IPFM) model, to achieve confidence, secondly, to a set of real HRV short-term data obtained during controlled breathing conditions, and, finally, to an HRV series involving non-stationary conditions.

2 Empirical mode decomposition (EMD)

The EMD relies on the decomposition of the original time series into component parts known as instantaneous mode functions (IMF), which are suitable for defining a meaningful instantaneous frequency (HUANG *et al.*, 1998). These functions are symmetric with respect to a local zero mean and have the same numbers of zero crossings and extrema. The extraction of these components is achieved by means of a decomposition based on the assumptions that the series has at least two extrema; that the characteristic time scale is defined by the elapsed time between extrema; and that, if the signal is unfilled by extrema but contains inflection points, a differentiation process applied once or more may reveal the extrema.

The decomposition method is essentially based on the identification of the extrema and on a sifting procedure in which an upper envelope is created by cubic spline interpolation of the local maxima; a lower envelope is created by interpolation of the local minima; and the difference between the original data $X(t)$ and the mean m_1 obtained from the upper and lower envelopes is designated as the first component C_1

$$C_1 = X(t) - m_1 \tag{1}$$

Ideally, this component will be an IMF; if it is not, new extrema can be generated, with the existing ones being either shifted or exaggerated. Thus this sifting procedure must be applied more than once to obtain an IMF. The aims of this repeated procedure are to eliminate the riding waves and to achieve a more symmetrical wave-profile by smoothing the uneven amplitudes. It is suggested (HUANG *et al.*, 1998) that a threshold is used, computed by summing the squared normalised differences from two consecutive sifting results, between 0.2 and 0.4 as a limit, to obtain the desired IMF first component. Once this condition is reached, the first component C_1 is subtracted from the original series $X(t)$ to leave the first residue R_1

$$R_1 = X(t) - C_1 \tag{2}$$

As this residue R_1 still contains information for longer scales, the decomposition procedure described above is then successively applied to the residue to obtain the next component. Each time a new component is reached, the new residual information is employed as the input information for the continuation of the procedure. Hence, the decomposition performs a general separation of the original signal into locally non-overlapping time scale components (or IMF).

To extract instantaneous frequency information for each of these IMF, the Hilbert transform is applied to each of the components to obtain the amplitude and the phase of the analytical signal of each component (HUANG *et al.*, 1998)

$$\begin{aligned} z(t) &= x(t) + iy(t) = a(t)e^{i\theta(t)} \\ a(t) &= \left[x^2(t) + y^2(t)\right]^{1/2} \\ \theta(t) &= \arctan\left(\frac{y(t)}{x(t)}\right) \\ w(t) &= \frac{d\theta(t)}{dt} \end{aligned} \tag{3}$$

where $y(t)$ is the Hilbert transform for any arbitrary time series $x(t)$; $z(t)$ is the analytical signal ($a(t)$ and $\theta(t)$ are, respectively, the amplitude and the phase of the analytical signal); and $w(t)$ represents a definition for the instantaneous frequency. Finally, by means of the combination of the amplitude and the derivative of the phase (i.e. the instantaneous frequency) of each component, it is possible to obtain the resulting amplitude, time-frequency, representation of the original series (HUANG *et al.*, 1998)

$$x(t) = \mathrm{Re}\,al\left\{\sum_{j=1}^{n} a_j(t)\exp\left(i\int w_j(t)dt\right)\right\} \tag{4}$$

where the subscript j is used to indicate the amplitude and phase obtained by means of the Hilbert transform on each j component of the EMD.

3 Data to be analysed

To assess the application of the EMD and the Hilbert transform, three simulated HRV series produced by the IPFM model, a chirp multicomponent signal, a set of real HRV short-term data obtained during controlled breathing condition and an HRV series involving non-stationary conditions, were selected.

3.1 *IPFM model*

This model has been used extensively to reproduce event series of modulated heart periods under simplified autonomic regulation conditions (DE BOER *et al.*, 1985; BERGER *et al.*, 1986; STEENIS *et al.*, 1994; NAKAO *et al.*, 1997). The model, originally presented by BAYLY (1968), transforms a continuous input signal into an event series representing the timings of cardiac activity. The input signal ($m_o + m(t)$), which involves a DC component (m_o) and a modulating sinusoidal component ($m(t)$), is integrated, and, whenever the integrated value exceeds a fixed threshold R, a unitary spike is generated, and the integrator is reinitialised. The integrated signal is identified with the membrane potential of the sinus node cells, which rises until the threshold is reached and an action potential is generated; the modulating sinusoidal input, generally involving two components to simulate the influences of the two autonomic limbs, represents the neural influences on the cells.

3.1.1 *Stationary simulated HRV data:* A composite sinusoidal input containing two frequency components of figures 0.12 Hz and 0.16 Hz, and magnitudes 0.3 and 0.2, respectively, was applied to the IPFM model, which generated a simulated heart beat events series, with a value 1.05 as a threshold and 1.0 as the DC component

$$m(t) = 0.3\,\cos(2\pi(0.12)t) + 0.2\,\cos(2\pi(0.16)t) \tag{5}$$

These settings were in accordance with the ones reported by DE BOER *et al.* (1985), except for the amplitude of the high-frequency component being 0.2 (i.e. 20% of deviation from the mean heart rate) rather than 0.3, in order to have different amplitude values for the low- and high-frequency components and to enable these values to be distinguished. From this series, a regularly sampled (4 Hz) R-R interval signal (shown at the top of Fig. 1), with a Nyquist frequency considerably above the frequency range of the input components (TASK FORCE, 1996), was constructed by means of a cubic spline interpolation.

3.1.2 *Non-stationary simulated HRV data (changing amplitude):* To explore the potential time-frequency tracking capabilities of the EMD and the associated Hilbert transform,

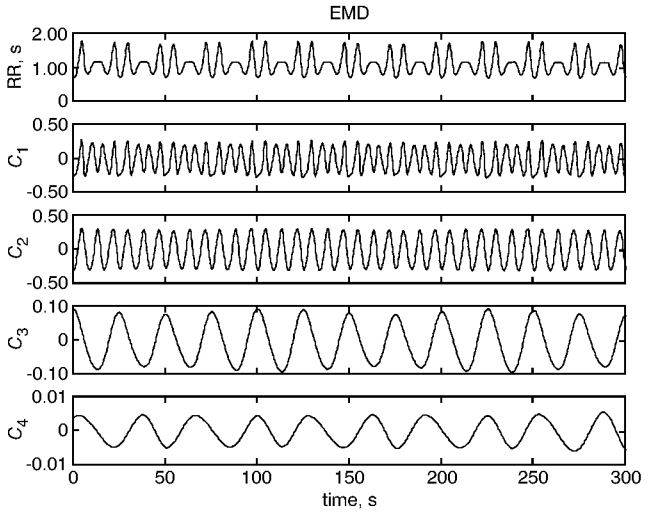

Fig. 1 *Results of EMD for an IPFM simulated series with following settings: $m(t) = 0.3\ cos(2\pi(0.12)t) + 0.2\ cos(2\pi(0.16)t$; 1.05 = threshold value; and 1 = DC input component. Top graph presents original series, and C_1–C_4 are first four extracted components using EMD*

a partial high-frequency blockage, simulating a simplified shift in the autonomic balance, was produced by changing the amplitude of the high-frequency component A_h from 0.3 to 0.15 during an IPFM simulation, with 1.05 as a threshold value, 1 as the DC input component, and the following composite sinusoidal input:

$$m(t) = 0.3\,\cos(2\pi(0.1)t) + A_h\,\cos(2\pi(0.21)t) \tag{6}$$

The above frequency values for the low- (0.1 Hz) and high-frequency (0.21 Hz) components were selected to produce different settings from the ones selected for the series in Section 3.1.1 (to demonstrate the potential of the EMD to extract these frequencies), and the other parameters of the simulation were chosen in accordance with the parameters reported by DE BOER *et al.* (1985).

Using this new event series, an R-R interval regularly sampled at 4 Hz signal (shown at the top of Fig. 2) was constructed by means of a cubic spline interpolation.

3.1.3 *Non-stationary simulated HRV data (changing frequencies):* To explore the capabilities of the EMD and the associated Hilbert transform for tracking changing frequencies on the main components, a change in the frequency value of the low-frequency component f_l from 0.1 to 0.12 Hz and a change in the frequency value of the high-frequency component f_h from 0.16 to 0.21 Hz were performed at the same time, during an IPFM simulation with 1.05 as a threshold value, 1 as the DC input component and the following composite sinusoidal input:

$$m(t) = 0.3\,\cos(2\pi(f_l)t) + 0.3\,\cos(2\pi(f_h)t) \tag{7}$$

The spline interpolated R-R interval signal at 4 Hz derived from this simulation is presented at the top of Fig. 3.

3.1.4 *Non-stationary simulated standard data (changing frequencies):* To explore further the EMD and the associated Hilbert transform for tracking changing frequencies, a chirp multicomponent signal was employed. This signal, presented at the top of Fig. 4, involves one component whose frequency linearly increases with time and a second component whose frequency linearly decreases at a different rate. The absolute

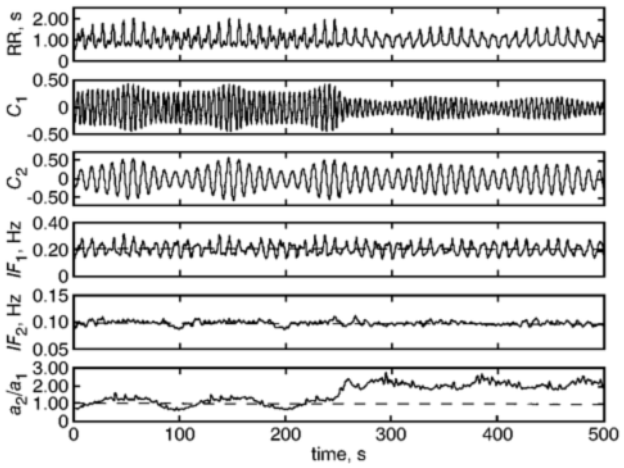

Fig. 2 *Results of EMD for IPFM simulated series with following settings: $m(t) = 0.3\ \cos(2\pi(0.1)t) + 0.3\ \cos(2\pi(0.21)t)$; 1.05 = threshold value; and 1 = DC input component. At 250 s, an amplitude change from 0.3 to 0.15 was introduced for high-frequency component. Top graph presents original series, and C_1, C_2 are used to describe first two components obtained by EMD. IF_1 indicates instantaneous frequency of C_1 component, and IF_2 is instantaneous frequency of C_2. Plot in bottom graph represents Hilbert amplitude ratio between second and first components; (- - - -) ratio of 1*

maximum amplitude of both components was equally established at unity. The initial and target components' frequencies were, respectively, selected in the recognised HF and LF HRV bands (TASK FORCE, 1996). In addition, the time to reach the frequency target for both components was selected to represent a recognised HRV short-term evolution. The initial frequency of the first component was selected to be 0.1857 Hz, and the target frequency was selected to be 0.3643 Hz, whereas the initial frequency of the second component was selected at 0.1343 Hz, and the target frequency

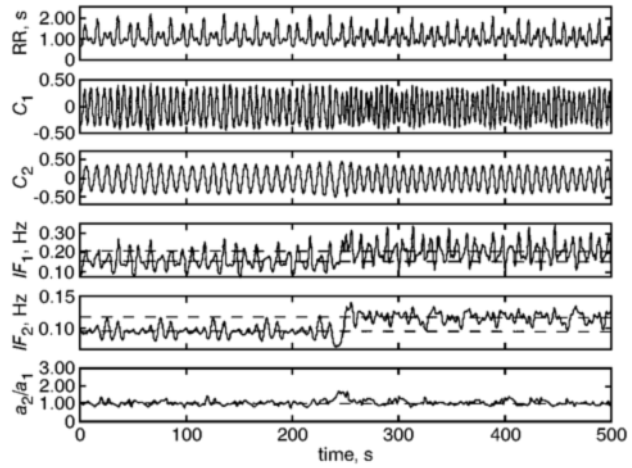

Fig. 3 *Results of EMD for IPFM simulated series with following settings: $m(t) = 0.3\ \cos(2\pi(f_l)t) + 0.3\ \cos(2\pi(f_h)t)$; 1.05 = threshold value; and 1 = DC input component. At 250 s, a frequency value change from 0.1 to 0.12 Hz was introduced for low-frequency component f_l, and a change from 0.16 to 0.21 was produced for high-frequency component f_h. Top graph presents original series, and C_1, C_2 are used to describe first two components obtained by EMD. IF_1 indicates instantaneous frequency of C_1 component, and IF_2 is used for instantaneous frequency of C_2. IF_1 graph: (- - - -) 0.10 and 0.12 values; IF_2 graph: (- - - -) 0.16 and 0.21. Plot in bottom graph represents Hilbert amplitude ratio between second and first components; (- - - -) ratio of 1*

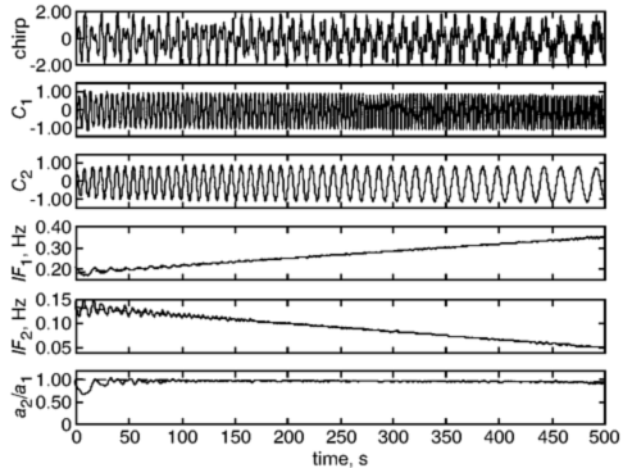

Fig. 4 *Results of EMD for multicomponent chirp signal having a frequency component increasing from 0.1857 to 0.3643 Hz and a frequency component decreasing from 0.1343 to 0.0557 Hz as settings during time window of 500 s. Top graph presents original series, and C_1, C_2 are used to describe first two components obtained by EMD. IF_1 indicates instantaneous frequency of C_1 component, and IF_2 is instantaneous frequency of C_2. IF_1 and IF_2 graphs: (- - -) least-square fitted lines. Plot in bottom graph indicates Hilbert amplitude ratio between second and first components; (- - -) ratio of 1*

was 0.0557 Hz at the final time, in both cases, of 500 s. The signal's sampling rate was set to be equal to 4 Hz.

3.2 *Real 'stationary' data*

To examine the new techniques on real data, a set of 14 real HRV signals, with 2 ms of resolution, of healthy subjects (nine women and five men; age range 20–35, mean 25) during short-term controlled metronomic breathing at 0.25 Hz was gathered from PhysioNet (GOLDBERGER *et al.*, 2000). Based on these event series and a cubic spline interpolation, regularly sampled (4 Hz) R-R interval signals, 5 min long, were generated (TASK FORCE, 1996). An example of these signals is presented at the top of Fig. 5.

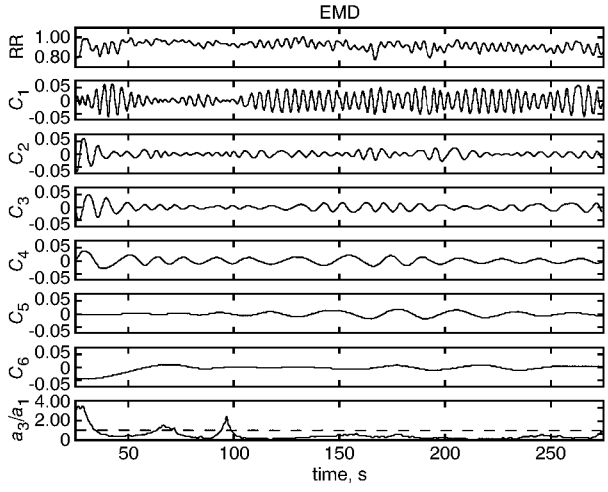

Fig. 5 *EMD of real short-term HRV signal from healthy young adult during controlled breathing at 0.25 Hz. Top graph presents original R-R interval series (s), and C_1–C_6 are used to describe first six components obtained by EMD. Plot in bottom graph represents Hilbert amplitude ratio between third and first components; (- - -) ratio of 1*

3.3 *Real 'non-stationary' data*

Finally, to evaluate the EMD and the Hilbert transform on an HRV signal involving transient phenomena, a short-term series was derived from a 500 Hz sampled ECG (TASK FORCE, 1996) of a young man (aged 29). The subject was seated, at rest, for 5 min, then actively stood up and remained in this upright position without movement for the last 6 min of the manoeuvre. The QRS fiducial points were detected by a standard 'band-pass, derivative and threshold' algorithm (TASK FORCE, 1996) and were regularly interpolated at 4 Hz using a cubic spline procedure (TASK FORCE, 1996). This signal is presented at the top of Fig. 6.

4 Results

The EMD was applied to the data series described in Section 3.1.1, and the Hilbert transform was calculated for the first three components of this decomposition. Then, the instantaneous frequency, i.e. the derivative of the phase of the analytical signal, of each component (C_1–C_3) was calculated according to eqns 3. Fig. 1 presents the results of the EMD on the simulated R-R interval; Fig. 7 involves the instantaneous frequency representation for these components.

The amplitudes of the C_1 and C_2 components are related to those (0.2 and 0.3) of the two sinusoidal inputs to the IPFM model, as are the centre values of the instantaneous frequency of these components (Fig. 7), which oscillate around 0.16 Hz and 0.12 Hz, respectively, thus being associated with the modulating frequency of the settings. Clearly, the component C_1 of the decomposition is identified as the high-frequency component of the IPFM sinusoidal input (i.e. $0.2\cos(2\pi(0.16)t)$), and the C_2 component is identified as the low-frequency component of the sinusoidal input (i.e. $0.3\cos(2\pi(0.12)t)$); nevertheless, it is possible to appreciate a more significant wave-profile distortion in the C_1 component than in the extracted C_2.

Also evident in Fig. 7 is a different excursion in the instantaneous-frequency representations of C_1 and C_2 that is related to the described wave-profile distortion in spite of the very similar amplitude settings (see Section 5). Additionally, a C_3 component, with lower, but not insignificant, amplitude, was

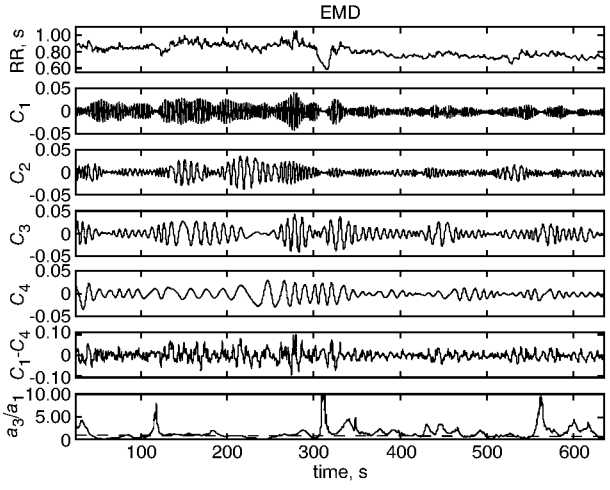

Fig. 6 *EMD of real short-term HRV signal from healthy young adult involving standing up movement at 300 s. Top graph presents original R-R interval series (s), and C_1, C_2, C_3, C_4 are used to describe first four components obtained by EMD. Also shown is reconstructed (C_1–C_4) series obtained by first four components of decomposition. Plot in bottom graph represents Hilbert amplitude ratio of third and first components; (- - -) ratio of 1*

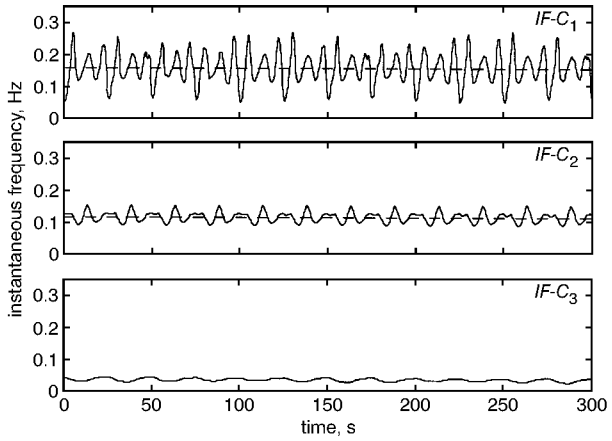

Fig. 7 *Instantaneous frequency for first three EMD components of Fig. 1. (- - -) 0.16 Hz and 0.12 Hz values*

produced by the EMD. According to the instantaneous-frequency results of Fig. 7, the mean frequency of this C_3 component is approximately 0.04 Hz, i.e. the difference between the two main frequencies. Finally, a C_4 component with a significantly lower amplitude was also generated by the EMD. This component may be an artefact due to the repetition of several spline fittings in the EMD sifting procedure (HUANG *et al.*, 1998); besides, as each successive IMF component of the EMD is obtained through the mean computed via the envelopes, a small leakage is always unavoidable (HUANG *et al.*, 1998).

The first two components extracted when the EMD is applied to the high-frequency blockage simulation series described in Section 3.1.2 are presented in Fig. 2, with their instantaneous frequencies. At the time 250 s, an amplitude change from 0.30 to 0.15 was introduced in the simulation for the high-frequency component. It is possible to observe this modification clearly in the C_1 component of Fig. 2. The change in amplitude was not present in the C_2 component. The instantaneous-frequency representations included in Fig. 2 act as verification that EMD components C_1 and C_2 again relate to the two IPFM inputs. Clearly, C_1 corresponds to the high-frequency setting, whose amplitude was intentionally reduced, whereas the C_2 component corresponds to the low-frequency contents of the IPFM input, whose amplitude was kept constant during the entire simulation.

To produce a time-tracking frequency distribution index, a ratio, referred to as the Hilbert amplitude ratio, was defined by dividing the amplitude of the analytical function of the low-frequency component C_2 by the amplitude of the analytical function of the high-frequency component C_1; the plot in the bottom graph of Fig. 2 represents this ratio as a function of time (a ratio reference value of one, i.e. the same amplitude for the analytical function of both components, is indicated by the broken horizontal line). Observing the ratio before and after the transition involving the instantaneous reduction of the amplitude of the high-frequency component, it is possible to note the clear increase in this ratio following the transition.

The first two components extracted when the EMD is applied to the simulation involving changing frequencies on the two main components of the series described in Section 3.1.3 are presented in Fig. 3, with their instantaneous frequencies. At the time 250 s, frequency changes from 0.1 to 0.12 Hz for the low-frequency component and from 0.16 to 0.21 for the high-frequency component were introduced in the simulation. It is possible to appreciate these transitions by means of the instantaneous-frequency representations included in Fig. 3. In this Figure, it is clearly shown that the component C_1 corresponds to the high-frequency setting, fluctuating around the mean frequency value of 0.16 Hz before and 0.21 Hz after the

transition, whereas the C_2 component corresponds to the high-frequency contents of the IPFM input, fluctuating around the mean frequency value of 0.10 Hz before and 0.12 Hz after the transition.

Although the simulated changes in the frequency of the two main components can be appreciated in both instantaneous-frequency representations, the transition is more easy to follow in the instantaneous-frequency representation of C_2, owing to the fact that excursion of this component is smaller, reflecting a lower wave-profile distortion (see Section 5). It is also possible to appreciate, as was expected, that the behaviour of the Hilbert amplitude ratio in the bottom graph of Fig. 3, defined by dividing the amplitude of the analytical function of the low-frequency component C_2 by the amplitude of the analytical function of the high-frequency component C_1, does not reflect a major change for the distribution of Hilbert amplitudes before and after the transition for the main components. Nevertheless, it is possible to detect a brief event (a ratio value greater than one) reflecting a temporarily alteration in this distribution during the transition.

Fig. 4 presents the results for the two main components of the decomposed chirp signal presented in Section 3.1.4. Clearly, it is shown that C_1 corresponds to the chirp's component whose frequency increases with time, whereas C_2 represents the component involving a decreasing frequency with time. A least-square line was fitted to the instantaneous-frequency representation of the first and second components. These results, shown as broken lines in Fig. 4, are in accordance with the original settings of the chirp signal: the intercepts for the first and second components are 0.1857 and 0.1344 Hz, respectively, which are precisely the initial frequencies of the settings. The slope for the first component is $3.5718 \times 10^{-4}\,\mathrm{Hz\,s^{-1}}$, which is very similar to the original chirp settings (0.01% absolute error difference), and the slope for the second component is $-1.5748 \times 10^{-4}\,\mathrm{Hz\,s^{-1}}$, again close to the original settings (0.22% absolute error difference). Furthermore, it is also possible to appreciate, in Fig. 4, particularly by means of the Hilbert amplitude ratio presented in the bottom graph, a larger wave-profile distortion at the beginning of the test where the two components have similar frequencies.

The interpolated real signals under controlled breathing conditions, presented in Section 3.2, were decomposed by the EMD, and the instantaneous frequency of each component was also calculated. In addition, the Hilbert amplitude ratio of C_3/C_1 (involving the central frequencies corresponding to the conventional LF/HF ratio) was also determined. An example of the results of the EMD for these real signals is presented in Fig. 5. Note that C_1, C_2, C_3 and C_4 have amplitudes of the same order, although the amplitude of C_1, which is related to the power concentration due to the controlled breathing, is predominant.

The final trace in Fig. 5 shows the Hilbert amplitude ratio between the third and first components. Its value, below one during most of the record, reflects the high-frequency predominance of the controlled breathing condition. The periods where the ratio goes above one suggest moments where the regular breathing pattern was not completely followed.

The power spectral density of the six components is presented in Fig. 8. It can be seen that the frequency excursions of C_2 and C_4, in particular, are not wholly contained within the currently recognised autonomic spectral bands (i.e. the low-frequency band from 0.04 to 0.15 Hz, and the high-frequency band from 0.15 to 0.4 Hz (TASK FORCE, 1996)). However, to complete a detailed analysis of the frequency behaviour of the components as a function of time, it is necessary to employ the instantaneous-frequency representation, obtained by means of the Hilbert transform, that is presented in Fig. 9. Here, changing frequencies for the components can be noticed, and the overlap of the recognised autonomic bands is even more evident for the excursions of the C_2 and C_4 components.

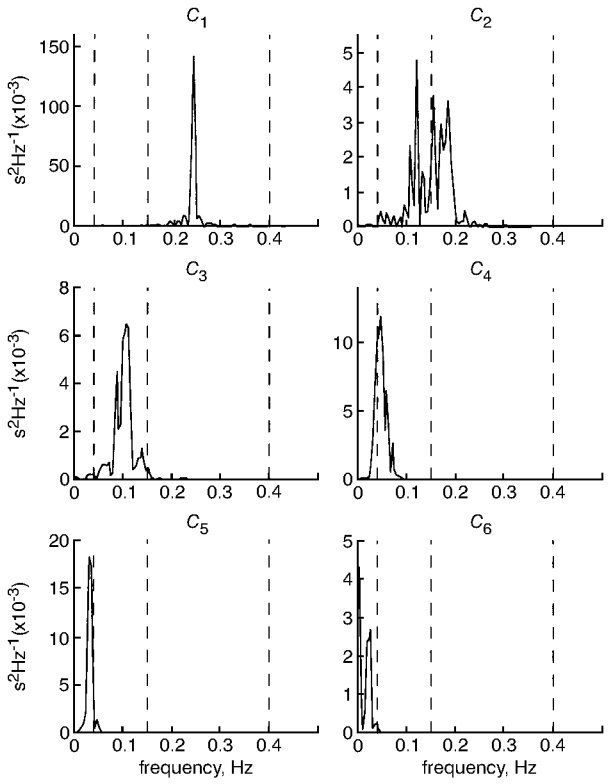

Fig. 8 *Power spectral density of first six components presented in Fig. 5. (- - -) Graphic delimitation of low- and high-frequency autonomic spectral bands at 0.04, 0.15 and 0.40 Hz*

Furthermore, according to the conventional delimitation of the spectral autonomic band, it is possible to appreciate that the high-frequency band involved the expected component that can be related to the controlled breathing frequency as well as an additional component. Although the contribution of this component is not very relevant for the conventional overall power quantification of the HF band, the possibility of isolating it from the rest of the band may indicate information with physiological significance.

In general, the application of the EMD on the 14 real controlled breathing signals consistently produced the isolation of at least four main components, with frequency excursions localised in the current recognised spectral bands of the autonomic modulation.

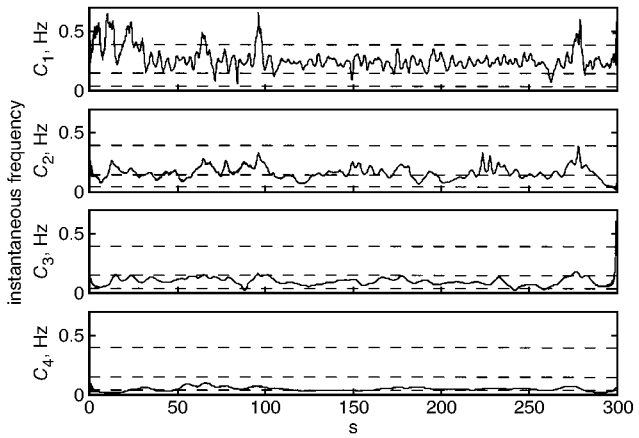

Fig. 9 *Instantaneous frequency as function of time for first four components presented in Fig. 5. (- - -) Graphical delimitation of current recognised autonomic spectral bands at 0.04, 0.15 and 0.40 Hz*

To illustrate the elimination of the non-autonomic contents of the HRV by means of the EMD, the left-hand side of Fig. 10 presents the traditional power spectral representation for the original R-R series of Fig. 5, obtained by means of a non-parametric calculation (the windowed FFT was applied after the original DC of the series had been removed) (TASK FORCE, 1996). Fig. 10*b* presents the traditional power spectral representation for the reconstructed series, adding only the first four components of the decomposition. It is possible to observe the elimination of the very low-frequency contents through this reconstruction.

The real series (described in Section 3.3) involving the transitory phenomena (standing up movement) was decomposed by the EMD and is presented in Fig. 6. In addition, Fig. 6 also presents the Hilbert amplitude ratio between the corresponding low-frequency component C_3 and the high-frequency component C_1. It is possible to identify the transitory event of this series at 300 s (top of the Figure), which would make it inappropriate to apply the traditional methods of frequency analysis; however, using the results of the new techniques, it is possible to examine the series by means of the reconstructed series (i.e. adding $C_1+C_2+C_3+C_4$ of the EMD, also presented in Fig. 6 and labelled C_1–C_4), where the non-linear trends have been filtered, or by means of the Hilbert autonomic ratio presented in the bottom plot. The transitory event was followed by this ratio, and the values of the ratio after this event indicate a different distribution, i.e. probably new autonomic conditions, for the rest of the manoeuvre. Besides, after this event, a different behaviour for the instantaneous-frequency representations of the first four components can also be appreciated in Fig. 11, perhaps showing a shift to higher frequencies during the upright position in all of the components.

5 Discussion

The results of the application of the EMD and the Hilbert transform to the IPFM simulated series, involving a composite sinusoidal input with two frequency components, demonstrate how these techniques enable the isolation of both original main modulating components. The amplitude of the C_1 and C_2 EMD components is related to the composite sinusoidal input of the

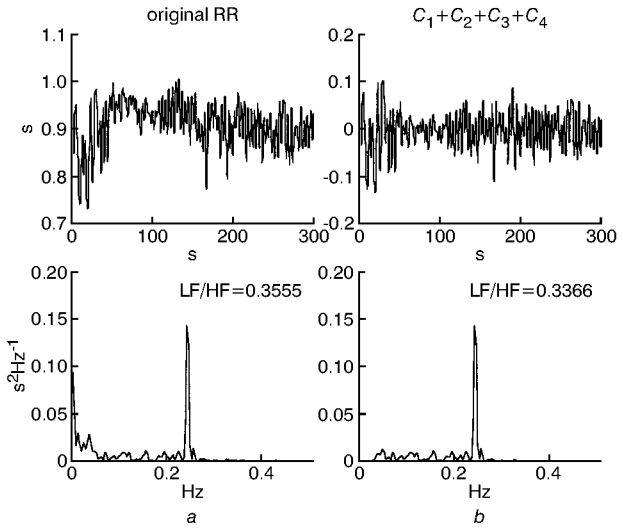

Fig. 10 *(a) Traditional power spectral representation for original R-R series of Fig. 5 (presented here again for clarity). (b) Traditional power spectral representation for reconstructed series obtained by first four components of decomposition shown in Fig. 5. Notice elimination of very low-frequency components*

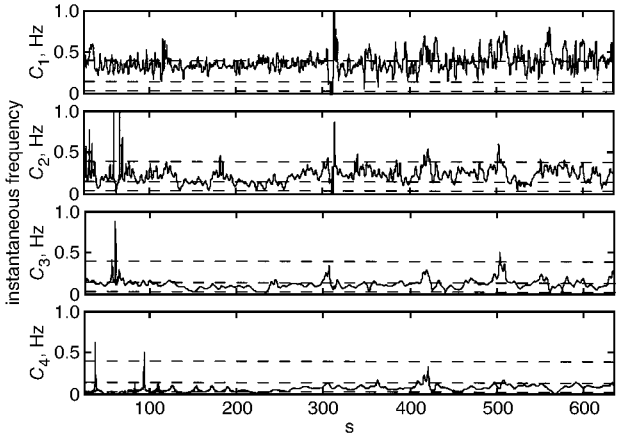

Fig. 11 *Instantaneous frequency as function of time for first four components presented in Fig. 6. (- - -) Graphical delimitation of current recognised autonomic spectral bands*

IPFM model, and the mean value of the instantaneous frequency of these components (Fig. 7) is associated with the modulating frequency of the settings. Additionally, a C_3 component with lower, but not insignificant, amplitude was also produced by the EMD.

According to NAKAO *et al.* (1997), when two components coexist in the IPFM input, additional interference components, which are not produced by the individual inputs, appear in the output of the IPFM. In the spectral representation obtained from the IPFM events series by means of the spectrum of counts, this non-linear interference, which depends on the IPFM settings, is presented as harmonic distortions that can occur in all the possible combinations of the main input frequencies. Given the instantaneous frequency results of Fig. 7, the mean frequency of the C_3 component is approximately 0.04 Hz, which is a value that can be obtained by a combination (i.e. the difference (DE BOER *et al.*, 1985)) of the two main frequencies, 0.12 and 0.16 Hz. Hence, using the EMD it was apparently also possible to recover the recognised (DE BOER *et al.*, 1985; NAKAO *et al.*, 1997) non-linear interference embedded in the IPFM output.

NAKAO *et al.* (1997) have pointed out that this non-linear effect depends on the IPFM input settings and, even if few dominant frequencies are introduced in the IPFM input, the resulting interference could produce harmonics over a wide frequency range. Moreover, a very different excursion was also found (Fig. 7) for the instantaneous frequency (IF) of C_1 and C_2 (in spite of the very similar amplitude settings), owing to a different wave profile distortion.

Before proceeding with this preliminary interpretation, it is convenient to discuss the theoretical meaning of the IF and how we obtained it, as several other approaches have also been proposed for the analytical signal phase derivative estimation of monocomponent signals (BOASHASH, 1992).

According to COHEN (1995), it is natural to define the IF as the derivative of the phase of the analytic signal, because its average over time is the average frequency. Therefore it is possible to consider the IF as the average of the frequencies existing at a particular time; the conditional standard deviation about this average, or the instantaneous band-width, is then related to the spread of frequencies at a particular time. Consequently, HUANG *et al.* (1998) proposed that, to obtain a meaningful IF, restrictive conditions have to be imposed on the data: the series must be locally symmetric with respect to the zero mean level, as well as having the same number of zero crossings and extrema. The intrinsic mode functions derived from the original data by the EMD procedure meet these restrictions and, hence, allow the calculation of the IF by means of the simple derivative of

the phase of the analytical signals of these functions (HUANG *et al.*, 1998).

According to HUANG *et al.* (1988), the conditions under which spurious harmonics are generated in the traditional Fourier analysis are non-linearity and non-stationarity. In their new method (EMD, Hilbert transform), these distortions are reflected in the IF as an intrawave modulation (i.e. any profile deformation within a wave), and they consider that this modulation has a clearer meaning from a physical point of view. Therefore, taking this assumption for the case of an IPFM derived series, it is possible to presume that the excursion of the IF is related to the amount of distortion produced by the combination of the IPFM original settings.

Theoretically and experimentally, it has been shown (BAYLY, 1968; DE BOER *et al.*, 1985; STEENIS *et al.*, 1994) that, in the spectral representation of events series produced by an IPFM model, a side-band distortion that can obscure the desired spectrum in the lower-frequency range is present. This distortion has been modelled as new harmonics in the analytical expressions derived by BAYLY (1968) and NAKAO (1997). The distortion is dependent on the mean heart rate R, the modulation amplitude m_A and the modulation frequency (DE BOER *et al.*, 1985; STEENIS *et al.*, 1994), with more distortion occurring for larger modulation depths (i.e. m_A/R) and higher modulation frequencies.

Consequently, and in summary, the results of Fig. 7 also suggest the use of the excursion of the instantaneous frequency to unmask and quantify the IPFM spectral distortion, perhaps owing to the inherent non-linearities of the model, that are present even when a simple (one-component) sinusoidal input to the model is selected. At present we are exploring this possibility.

The application of the EMD to the 14 real signals consistently produced the isolation of at least four main components (C_1, C_2, C_3 and C_4) with comparable amplitudes (Fig. 5), and, as illustrated in the Fourier and instantaneous-frequency spectral representations of Figs 8 and 9, with overlapping frequency excursions localised in the currently recognised spectral bands of the autonomic modulation. According to HUANG *et al.* (1998), one of the most remarkable considerations of the EMD method is that the meaning of the produced components can be physical (or for these data, physiological), rather than the traditional orthogonal meaning associated with the linear decompositions; therefore the finding of these independent autonomic components for the real HRV series may be extremely important: it seems that, with traditional frequency analysis, these components are merged, perhaps because of the practical, yet arbitrary, delimitation of the spectral bands (when using non-parametric methods), or because of the lack of sensitivity due to the extreme dependence in the selection of the model order by spectral parametric methods.

On the other hand, it seems that, by the reconstruction of the real HRV series under short-term conditions using the first four components of the EMD, it was possible to recover the autonomic power that was masked by the very low-frequency contents (Fig. 10). This can be confirmed in the different value of the ratio (LF/HF) after the reconstruction. Besides, for the case of the manoeuvre involving the standing up movement (Fig. 6), this reconstruction (C_1–C_4) filtered the trends, specifically the non-linear ones around the transition at 300 s.

The definition of the Hilbert amplitude ratio of two of the main autonomic components of the decomposition seems to be a convenient time tracking index for the frequency distribution in the HRV series, which may be adequate for the proper assessment of the dynamic and transient amplitude changes of the HRV components. This can be easily verified in the top and bottom plots of Figs 2 and 6, respectively, where the ratio indicated the high-frequency partial blockage simulation and was influenced by the transitory phenomena. In these Figures and in Fig. 5, it is clear that a ratio above one can be associated with the reduction of high-frequency oscillations in that particular zone of the original HRV trace. In contrast, a ratio below one can be associated with the loss of predominance of the low-frequency oscillations. In subsequent evaluations of this ratio, other combinations of the Hilbert amplitude for the main autonomic components should also be explored.

Finally, by means of the EMD and its associated Hilbert transform, it was also possible to detect, as a function of time, the changing frequencies of the components of the HRV. This can be noticed in the instantaneous-frequency representations of Fig. 3 reflecting the expected changes due to the simulation, in the representations of Fig. 11 that seem to reflect a shift to higher frequencies after the transition, and in the representations of Fig. 9 indicating a dynamic evolution for the main frequency components, in spite of the controlled breathing conditions for this real signal. Therefore these techniques appear to be useful, as well, for proper assessment of the dynamic frequency changes in the autonomic regulation. These capabilities for tracking frequency changes during short-term windows of time and in the HRV frequency bands were also verified by the frequency representations of the decomposed chirp signal. Additionally, the excursion of this instantaneous frequency and the Hilbert amplitude ratio revealed a very interesting distortion (which is perhaps more difficult to appreciate and evaluate via alternative techniques). A notorious intrawave modulation, perhaps reflecting a real non-linear distortion between components, is evident at the beginning of the test, where both components have similar frequencies.

6 Conclusions

By means of the EMD, it was possible to recover and isolate the original IPFM settings, including the non-linear interference present in the IPFM output. It has also been suggested that the excursion of the instantaneous frequency could be used as a way to unmask and quantify the spectral distortion; hence, subsequent studies of the behaviour of the instantaneous frequencies obtained from simulated and real HRV series should be relevant. In addition, for real HRV signals, the EMD permitted the isolation of at least four components with overlapping and dynamic frequency excursions localised in the currently recognised spectral bands of the autonomic modulation: it apparently permitted the separation of the very low-frequency contents as well. In addition, the definition of the Hilbert amplitude ratio using the main components of the EMD seems to produce a convenient time tracking index of the distribution of high- and low-frequency oscillations in the HRV spectrum (even in the presence of non-stationary conditions). Finally, the instantaneous-frequency representations appear to reveal accurately the frequency changes that can be found in HRV data.

In conclusion, the results of this paper suggest the use of the EMD and the associated Hilbert spectral representation as powerful techniques for HRV data time-frequency analysis, owing to the capabilities of independently isolating the main frequency components, the possibility of dealing with non-stationary and non-linear embedded phenomena, and perhaps owing to its suitability for a proper assessment of the dynamic and transient changes in amplitude and in frequency of the HRV components.

Acknowledgments—J.C. Echeverría acknowledges the financial support provided by the Mexican Council for Science & Technology (CONACyT).

References

BAYLY, E. (1968): 'Spectral analysis of pulse frequency modulation in the nervous systems', *IEEE Trans. Biomed. Eng.*, **15**, pp. 257–265

BERGER, R., AKSELROD, S., GORDON, D., and COHEN, R. (1986): 'An efficient algorithm for spectral analysis of heart rate variability', *IEEE Trans. Biomed. Eng.*, **33**, pp. 900–904

BOASHASH, B. (1992): 'Estimating and interpreting the instantaneous frequency of a signal-part 2: algorithms and applications', *Proc. IEEE*, **80**, pp. 540–568

BROWN, T., BREGHTOL, L., KOH, J., and ECKBERG, D. (1993): 'Important influence of respiration on human R-R interval power spectra is largely ignored', *J. Appl. Physiol.*, **75**, pp. 2310–2317

CHAN, H., LIN, J., HUANG, H., and WU, C. (1997): 'Elimination of interference component in Wigner-Ville distribution for the signal with 1/f spectral characteristic', *IEEE Trans. Biomed. Eng.*, **44**, pp. 903–907

COHEN, L. (1995): 'Time-frequency analysis' (Prentice Hall, Englewood Cliffs, NJ), pp. 1–43

COOKE, W., HOAG, J., CROSSMAN, A., KUUSELA, T., TAHVANAINEN, K., and ECKBERG, D. (1999): 'Human responses to upright tilt: a window on central autonomic integration', *J. Physiol.*, **517**, pp. 617–628

DE BOER, R., KAREMAKER, J., and STRACKEE, J. (1985): 'Spectrum of a series of point events, generated by the integral pulse frequency modulation model', *Med. Biol. Eng. Comput.*, **23**, pp. 138–142

ECHEVERRÍA, J., MEDINA, V., and CARRASCO, S. (1997): 'A comparison between the peak ear pulse derivative and the R-R interval variabilities', *Comput. Cardiol.*, **24**, pp. 445–447

ECKBERG, D. (1996): 'Sympathovagal balance. A critical appraisal', *Circulation*, **96**, pp. 3226–3232

GOLDBERGER, A., AMARAL, L., GLASS, L., HAUSDORFF, J., IVANOV, P., MARK, R., MIETUS, J., MOODY, G., PENG, C., and STANLY, E. (2000): 'PhysioBank, PhysioToolkit, and PhysioNet. Components of a new research resource for complex physiological signals', *Circulation*, **101**, pp. e215–e220

HUANG, N., SHEN, Z., LONG, S., WU, M., SHIH, H., ZHENG, Q., YEN, N., TUNG, C., and LIU, H. (1998): 'The empirical mode decomposition and the Hilbert spectrum for nonlinear and non-stationary time series analysis', *Proc. R. Soc. London*, **454**, pp. 903–995

KAREMAKER, J. (1999): 'Autonomic integration: the physiological basis of cardiovascular variability', *J. Physiol.*, **517**, p. 316

KOBAYASHI, M., and MUSHA, T. (1982): '1/f fluctuations of heartbeat period', *IEEE Trans. Biomed. Eng.*, **29**, pp. 456–457

MAINARDI, L., BIANCHI, A., BASELLI, G., and CERRUTI, S. (1995): 'Pole-tracking algorithm for the extraction of time-variant heart rate variability spectral parameters', *IEEE Trans. Biomed. Eng.*, **42**, pp. 250–259

MALLIANI, A., PAGANI, M., LOMBARDI, F., and CERRUTI, S. (1991): 'Cardiovascular neural regulation explored in the frequency domain', *Circulation*, **84**, pp. 482–492

NAKAO, M., NORIMATSU, M., MIZUTANI, Y., and YAMAMOTO, M. (1997): 'Spectral distortions properties of the Integral Pulse Frequency Modulation Model', *IEEE Trans. Biomed. Eng.*, **44**, pp. 419–426

SAUL, P., ALBRECHT, P., BERGER, R., and COHEN, R. (1988): 'Analysis of long term heart rate variability: methods, 1/f scaling and implications', *Comput. Cardiol.*, pp. 419–422

SCHECHTMAN, V., KLUGE, K., and HARPER, R. (1988): 'Time-domain system for assessing variation in heart rate', *Med. Biol. Eng. Comput.*, **26**, pp. 367–373

SHIN, S., TAPP, W., RESMAN, S., and NATELSON, B. (1989): 'Assessment of autonomic regulation of heart rate variability by the method of complex demodulation', *IEEE Trans. Biomed. Eng.*, **36**, pp. 274–283

STEENIS, H., TULEN, J., and MULDER, L. (1994): 'Heart rate variability spectra based on non-equidistant sampling: the spectrum of counts and the instantaneous heart rate spectrum', *Med. Eng. Phys.*, **16**, pp. 355–362

STEIN, P., and KLEIGER, R. (1999): 'Insights from the study of the heart rate variability', *Ann. Rev. Med.*, **50**, pp. 249–261

TASK FORCE EUROPEAN SOCIETY OF CARDIOLOGY AND NORTH AMERICAN SOCIETY OF PACING ELECTROPHYSIOLOGY (1996): 'Heart rate variability. Standards of measurement, physiological interpretation, and clinical use', *Europ. Heart J.*, **17**, pp. 354–381

YAMAMOTO, Y., and HUGHSON, R. (1991): 'Coarse-graining spectral analysis: new method for studying heart rate variability', *J. Appl. Physiol.*, **71**, pp. 1143–1150

Authors' biographies

JUAN ECHEVERRÍA was born in Mexico in 1970. He received his BSc and MSc in Biomedical Engineering from the Metropolitan Autonomous University of Mexico City, where he holds an academic position. Currently, he is on a PhD secondment in the School of Electrical and Electronic Engineering of the University of Nottingham. His research interests are the analysis of the cardiovascular beat to beat fluctuations and the antenatal evaluation of foetal heart rate variability.

JOHN CROWE, MALCOLM WOOLFSON and BARRIE HAYES-GILL all joined the University of Nottingham in the late 1980s as lecturers in Medical Electronics, Signal Processing and VLSI Design respectively. Since this time they have formed the core of the School of Electrical & Electronic Engineering's Biomedical Informatics Group and have collaborated internationally with clinicians, fellow engineers and industrial partners on numerous projects. These have included the design and construction of novel instrumentation for physiological monitoring, the telemetry of biomedical data and biomedical signal processing, of which this paper is one example.